

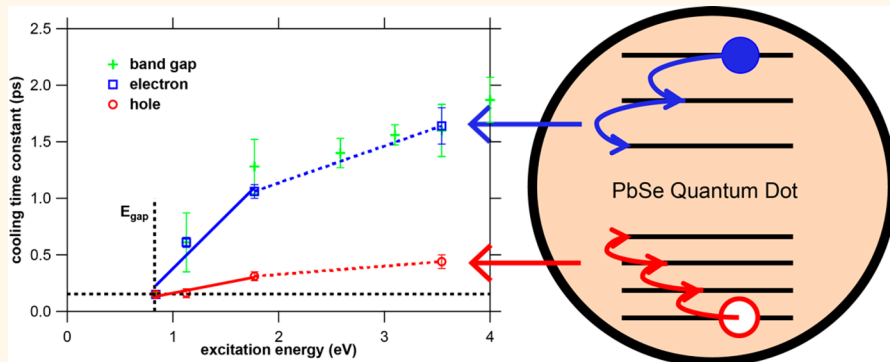
# Hole Cooling Is Much Faster than Electron Cooling in PbSe Quantum Dots

Frank C. M. Spoor,<sup>†</sup> Lucas T. Kunneman,<sup>†</sup> Wiel H. Evers,<sup>†,‡</sup> Nicolas Renaud,<sup>†</sup> Ferdinand C. Grozema,<sup>†</sup> Arjan J. Houtepen,<sup>\*,†</sup> and Laurens D. A. Siebbeles<sup>\*,†</sup>

<sup>†</sup> Optoelectronic Materials Section, Department of Chemical Engineering, Delft University of Technology, Julianalaan 136, 2628 BL Delft, The Netherlands

<sup>‡</sup> Kavli Institute of Nanoscience, Delft University of Technology, Lorentzweg 1, 2628 CJ Delft, The Netherlands

 Supporting Information



**ABSTRACT:** In semiconductor quantum dots (QDs), charge carrier cooling is in direct competition with processes such as carrier multiplication or hot charge extraction that may improve the light conversion efficiency of photovoltaic devices. Understanding charge carrier cooling is therefore of great interest. We investigate high-energy optical transitions in PbSe QDs using hyperspectral transient absorption spectroscopy. We observe bleaching of optical transitions involving higher valence and conduction bands upon band edge excitation. The kinetics of rise of the bleach of these transitions after a pump laser pulse allow us to monitor, for the first time, cooling of hot electrons and hot holes separately. Our results show that holes cool significantly faster than electrons in PbSe QDs. This is in contrast to the common assumption that electrons and holes behave similarly in Pb chalcogenide QDs and has important implications for the utilization of hot charge carriers in photovoltaic devices.

**KEYWORDS:** quantum dot, nanocrystal, transient absorption spectroscopy, charge carrier cooling, band structure, electron acceptor

The optical and electrical properties of colloidal semiconductor quantum dots (QDs) have been studied extensively due to their promising properties for use in devices such as field-effect transistors, light-emitting diodes, photodetectors and solar cells.<sup>1</sup> In photovoltaic devices, absorption of a photon leads to promotion of an electron from a valence band to a conduction band. The photon energy in excess of the band gap is divided over the hole in the valence band and the electron in the conduction band. The initially hot electron and hole can relax to the states at the band edge by releasing their excess energy as heat to the lattice. This process of charge carrier cooling limits the efficiency of photovoltaic devices. Several options exist to reduce the energy loss *via* cooling.<sup>2</sup> For instance, the voltage of a photovoltaic device can be enhanced by extracting hot carriers from the QD before cooling takes place.<sup>3–5</sup> Alternatively, the current can be enhanced by carrier multiplication (also known as multiple

exciton generation), in which a sufficiently energetic carrier excites a second (and possibly third, etc.) carrier over the band gap.<sup>6–9</sup> These two processes occur in competition with carrier cooling. Hence, understanding cooling in QDs will be useful to exploit hot carrier extraction and carrier multiplication in photovoltaic devices.

Previous studies of charge carrier cooling in QDs have mainly focused on energy levels near the valence and conduction band edges.<sup>10–13</sup> Less attention has been paid to cooling from electronic states at higher energies, for which it is commonly accepted that energy levels become more densely spaced and converge to a bulk-like electronic structure.<sup>14,15</sup> In addition, other relaxation pathways may become available as hot charge

**Received:** September 11, 2015

**Accepted:** December 10, 2015



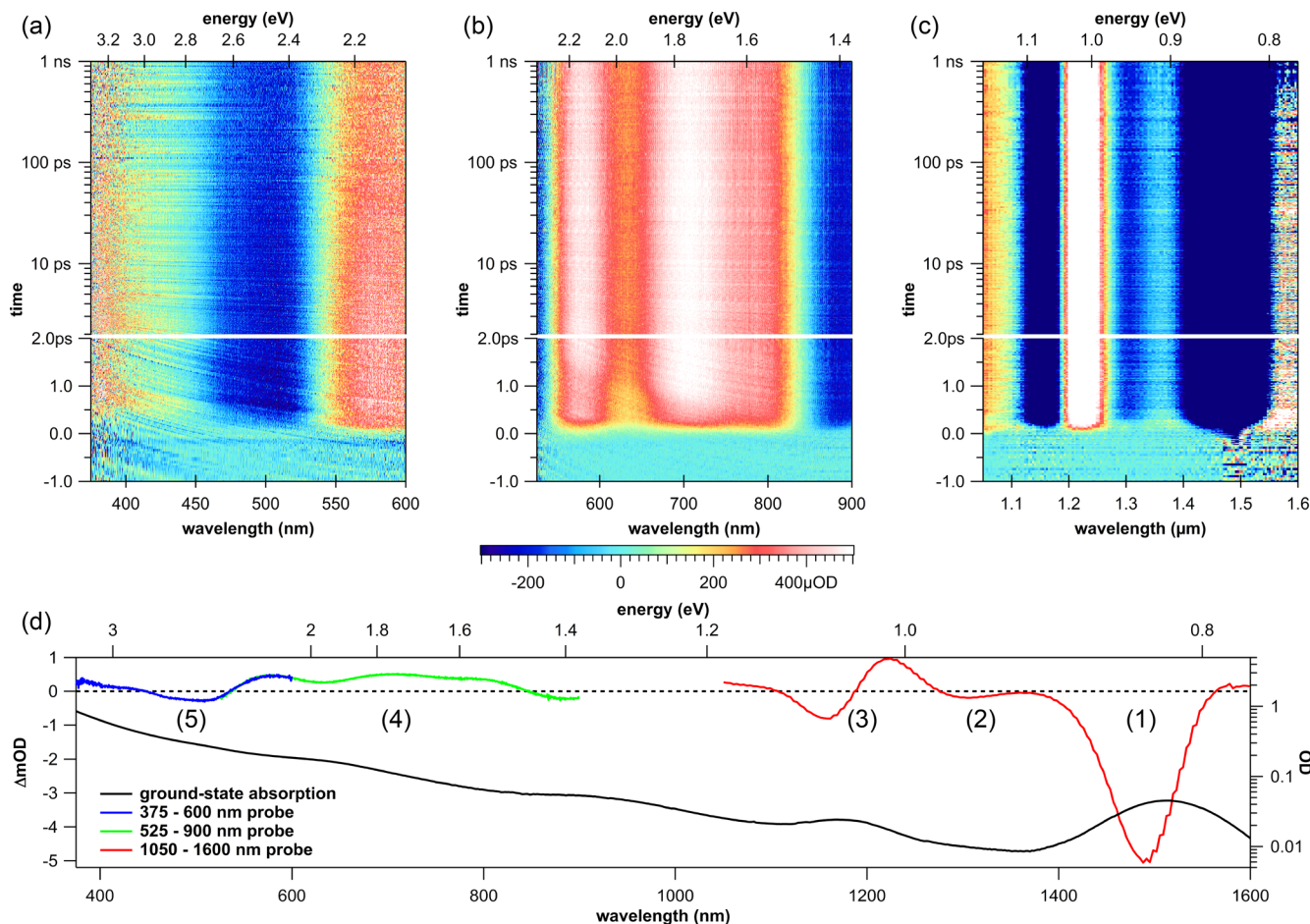


**Figure 1.** Hyperspectral TA image for 4.8 nm PbSe QDs excited by a pump laser pulse with photon energy at the band gap (0.83 eV, 1500 nm) and probed by a 375–600 nm (a), 525–900 nm (b), and 1050–1600 nm (c) broadband probe pulse. The TA images are corrected for dispersion in the probe light (see [Methods](#)). (d) Spectral slice taken from the TA images at 10 ps pump–probe delay, together with the ground-state absorption spectrum. The labeled features are discussed in the text.

carriers are created, as was shown for, *e.g.*, InP QDs.<sup>16,17</sup> The most studied QD material in the context of carrier multiplication<sup>8</sup> and hot carrier extraction<sup>3</sup> is PbSe. Research on charge carrier cooling in PbSe QDs has been performed using ultrafast optical pump–probe spectroscopy and focused mainly on relaxation from the first excited 1P electron/hole states down to the 1S states at the band gap, see, *e.g.*, refs 11, 12, 18–20 and references therein. These experimental studies yield a combined rate for electron and hole cooling. Rates for electron and hole cooling have often been assumed to be equal, due to the similar spacing between electron and hole energy levels near the band gap of PbSe QDs.<sup>21</sup> However, theoretical calculations,<sup>22</sup> scanning tunneling spectroscopy<sup>23</sup> and optical measurements<sup>18</sup> show that PbSe diverts from the suggested symmetric energy levels for electron and hole and that the hole level spacing is significantly denser. This may lead to increased hole cooling rates compared to electron cooling rates. However, to the best of our knowledge, information on the separate electron and hole cooling rates in PbSe has not been published until now.

We present a femtosecond pump–probe transient absorption (TA) study of electron and hole states involved in optical transitions in PbSe QDs at energies well above the band gap. First we create cold 1S<sub>h</sub>–1S<sub>e</sub> excitons by photoexcitation of PbSe QDs at the band gap and characterize the nature of transitions in the TA spectrum in the wavelength range of 375–

1600 nm. In addition to the optical bleach at the band gap, also energetically higher lying transitions are bleached. The latter transitions can be attributed to transitions to the second valence and conduction bands at the L-point in the Brillouin zone of PbSe. We utilize the knowledge of the nature of the high-energy optical transitions to separately determine the rates of electron and hole cooling as a function of photoexcitation energy. Our results show that hole cooling is much faster than electron cooling.

## RESULTS AND DISCUSSION

PbSe QDs of various sizes were prepared *via* the method described by Steckel *et al.*,<sup>24</sup> washed twice and dispersed in toluene (see [Methods](#)). The QD dispersions were investigated by TA spectroscopy with a time-resolution of ~180 fs and a probe spectral range of 350–1600 nm (see [Methods](#)). In [Figure 1](#) we show the hyperspectral TA image that results from probing in the wavelength range 375–600 nm (a), 525–900 nm (b), and 1050–1600 nm (c) for 4.8 nm PbSe QDs after excitation by a pump laser pulse with photon energy at the band gap (0.83 eV, 1500 nm), so that charge carrier cooling does not occur. In all experiments described below the pump laser fluence was sufficiently low that much less than one exciton per QD was created and Auger recombination of multiexcitons did not take place. The exciton lifetime in PbSe

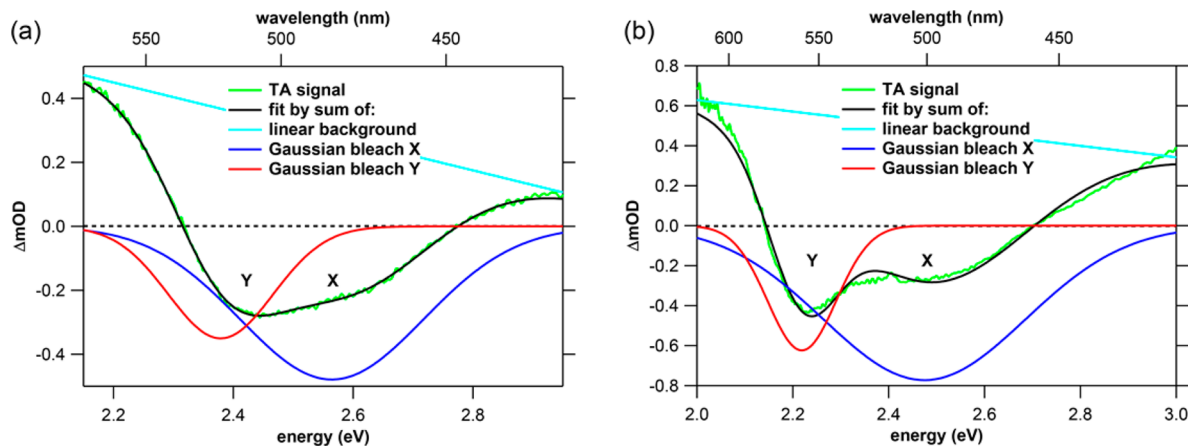


**Figure 2.** TA spectra at energies around the bleach features X and Y for 4.8 nm QDs (a) and 7.0 nm QDs (b). The TA spectra are well described by two Gaussian bleach features X and Y, superimposed on a positive background that decreases linearly with photon energy.

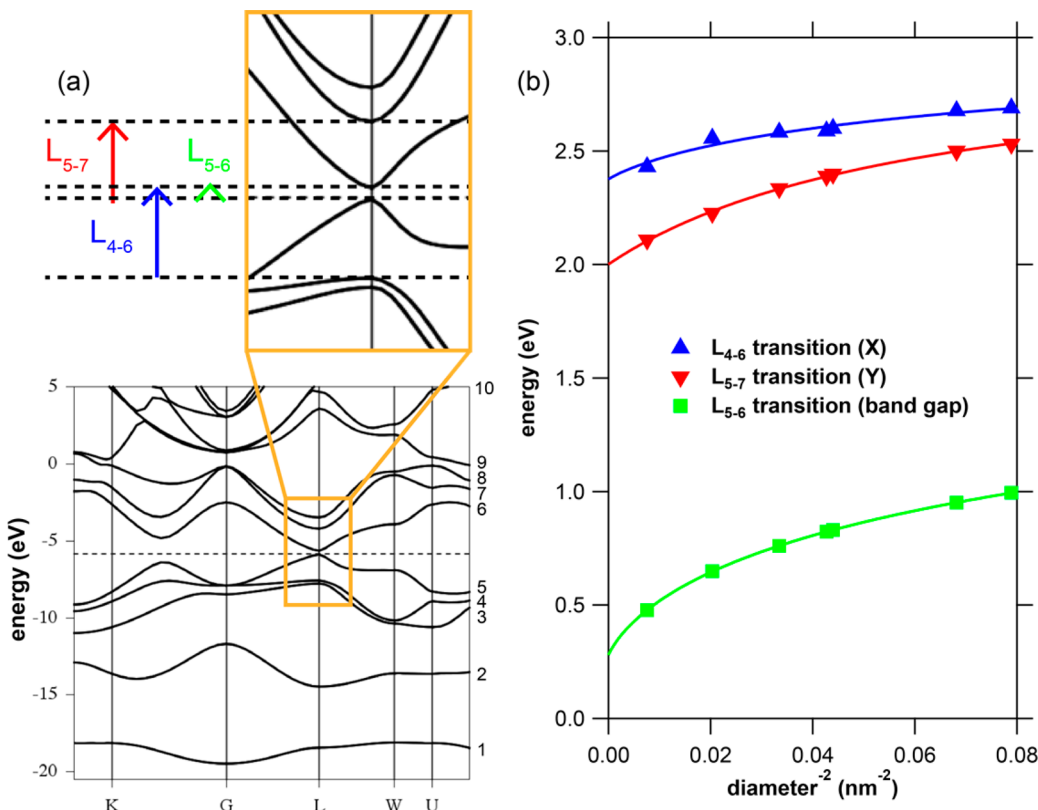


**Figure 3.** (a) PbSe bulk band structure calculated with DFT. The enlargement shows the relevant transitions at the L-point of the Brillouin zone. (b) Energies of the band gap and bleach features X and Y, determined from Gaussian fits to TA spectra as in Figure 2, versus the inverse square of the QD diameter. Fits of eq 1 to the energies of X and Y are shown as solid lines. At large diameter, the fitted energies of X and Y are close to the L<sub>4-6</sub> and L<sub>5-7</sub> transition energies calculated for bulk, see also Table 1.

QDs is several hundreds of nanoseconds,<sup>25,26</sup> so that the TA does not exhibit significant decay during the 1 ns time window considered. Figure 1d shows a spectral slice taken from the TA images at 10 ps pump–probe delay, together with the ground-state absorption spectrum. While features in the range 500–1600 nm of the TA image have been discussed in literature before,<sup>18,19,27</sup> those at short wavelengths were not discussed previously.

At the longest probe wavelengths, we observe a negative TA signal (1), or bleach, due to reduced ground state absorption and stimulated emission resulting from the presence of the

1S<sub>h</sub>–1S<sub>e</sub> exciton.<sup>28</sup> At shorter probe wavelengths, we observe a derivative-like feature (3), assigned to a red-shift of the 1P<sub>h</sub>–1P<sub>e</sub> transition resulting from biexciton interactions.<sup>18</sup> The small bleach (2) at intermediate wavelengths is due to the weak 1S<sub>h</sub>–1P<sub>e</sub> and 1P<sub>h</sub>–1S<sub>e</sub> transitions.<sup>19,20</sup> At wavelengths in the visible, we observe a broad positive TA signal (4) of photoinduced absorption (PA), recently attributed to a red-shift of the ground-state absorption spectrum due to biexciton interactions.<sup>29</sup>

At probe wavelengths approaching the UV, we observe another bleach signal (5) that has not been discussed in the

literature before. Figure 2 shows this bleach in detail for two QD sizes. The bleach can be considered to consist of two contributions, labeled X at higher photon energy and Y at lower energy, superimposed on a positive background. The positive background likely relates to a continuation of the broad PA feature labeled (4) in Figure 1d and possibly contains contributions from intraband absorption as well (see Figure S1 and related discussion in the Supporting Information). In Figure 2, we choose to describe the background as a linear function. The energy dependence of each of the bleach features X and Y can be described by a Gaussian function. These features cannot result from a biexciton red-shift, since at high photon energy the ground-state absorption spectrum increases monotonically with energy and consequently a biexciton red-shift would result in PA rather than bleach. Hence, the bleach features X and Y must originate from blocking of electronic transitions due to the presence of a  $1S_h$  hole and/or a  $1S_e$  electron at the band edge.

To investigate the nature of the high-energy bleach features X and Y, we computed the PbSe bulk band structure at the density functional level of theory (DFT) using the ADF/BAND program (see Methods).<sup>30–32</sup> Spin-orbit coupling was explicitly taken into account via a ZORA approach. The calculated band structure is shown in Figure 3a. We label the bands with indices 1–10 from the lowest to the highest energy and refer to electronic transitions according to the convention of Kohn *et al.*, see Figure 3a,<sup>33</sup> which implies that excitation at the band gap corresponds with the  $L_{5-6}$  transition. Higher lying conduction bands and lower lying valence bands have extrema at the L-point of the Brillouin zone as well. The lowest transitions in excess of the band gap that involve the band edge electron ( $L_{4-6}$ ) or band edge hole ( $L_{5-7}$ ) are optically allowed.<sup>33</sup> The energies of these transitions calculated for bulk PbSe are listed in Table 1. From the order of the transition

**Table 1. PbSe Bulk Transition Energies at the L-Point Obtained from DFT Calculations, Together with Those Obtained from Fitting Equation 1 to the Experimental Transition Energies for QDs<sup>a</sup>**

transition	calculated energy (eV)	fitted energy, $E_0$ (eV)	R
$L_{5-6}$	0.25	$0.28 \pm 0.001$	1.12
$L_{5-7}$	1.68	$2.00 \pm 0.01$	1.2
$L_{4-6}$	1.94	$2.38 \pm 0.02$	1.2

<sup>a</sup>R is the ratio of the fitted and calculated bulk transition energies.

energies, it is likely that the higher energy feature X for QDs in Figure 2 corresponds to the  $L_{4-6}$  transition, while the lower energy feature Y is likely due to the  $L_{5-7}$  transition.

When considering QDs instead of bulk, the energy of the transitions increases as the diameter of a QD becomes smaller due to quantum confinement. Figure 3b shows the measured band gap energy as well as the energies of the Gaussian bleach features X and Y as a function of the inverse square of the QD diameter. We used Gaussian fits as in Figure 2 to determine the energies of X and Y from the TA spectra. The energies of X and Y are size dependent, and the effect is somewhat stronger for Y. The dependence of the transition energies on the QD diameter  $D$  can be described as<sup>34</sup>

$$E(D) = E_0 + \frac{1}{(aD^2 + bD + c)} \quad (1)$$

(see the solid lines in Figure 3b). The bulk transition energies  $E_0$  obtained from fitting eq 1 to the data are listed in Table 1. The fitted energies exceed the DFT results by 20% or less. On the basis of the agreement between the fitted bulk transition energies and the DFT values, we assign bleach feature X to the  $L_{4-6}$  transition and bleach feature Y to the  $L_{5-7}$  transition.

We note that, in principle, several envelope functions ( $1S$ ,  $1P$ , ...) should be present within each band just as they are for the  $L_5$  and  $L_6$  bands near the band gap. Hence, the proper description of the transition responsible for feature X is  $L_41S_h - L_61S_e$ , while  $L_51S_h - L_71S_e$  denotes the transition that gives rise to feature Y. However, in these TA experiments, all bleach features are due to  $1S_h - 1S_e$  transitions in the various bands. For simplicity, we denote them  $L_{4-6}$ ,  $L_{5-7}$ , and  $L_{5-6}$  and stress that we consider  $1S$  envelope functions in all cases.

We observe from Figure 3b that the  $L_{4-6}$  transition energy (X) changes less with QD diameter than the  $L_{5-7}$  transition energy (Y). Table S1 in the Supporting Information shows the transverse and longitudinal effective masses calculated for bands 4–7 at the L-point, see Figure 3a. The effective masses of charge carriers in band 7 are lower than in band 4, while the effective masses in band 5 and 6 are comparable. This agrees with the stronger dependence of the  $L_{5-7}$  transition energy on QD diameter than the  $L_{4-6}$  transition, see Figure 3b.

To further corroborate the assignment of bleach feature X to the  $L_{4-6}$  transition and bleach feature Y to the  $L_{5-7}$  transition, we add methylene blue (MB) as electron acceptor to the QDs, in order to remove the  $1S_e$  ( $L_6$ ) electron after photoexcitation of the QDs at the band gap. The photogenerated  $1S_e$  electron will transfer to MB, leaving only the  $1S_h$  ( $L_5$ ) hole in the QDs. This process is schematically shown in Figure 4a. Eventually, the hole recombines with the transferred electron and the system returns to the ground state. Such electron transfer and electron–hole recombination has previously been demonstrated for CdSe and PbS QDs with MB.<sup>35,36</sup>

In Figure 4b we show the bleach transient at the  $L_{5-6}$  transition for 4.8 nm PbSe QDs without MB and with 5 MB molecules added per QD. Clearly, the addition of MB induces a decay of the  $L_{5-6}$  bleach, which can be described by a biexponential function with time constants of 1.5 and 10 ps. These values are comparable to those found for PbS QDs.<sup>36</sup> The exponential function with the short time constant describes electron transfer from QDs to MB, while the second exponential function describes subsequent electron–hole recombination of the electron on the MB molecule with the hole still residing in the QD. The complete disappearance of the bleach after several tens of picoseconds implies that all photoexcited electrons undergo electron transfer to MB, followed by electron–hole recombination. The amplitudes of the two exponential functions were free fitting parameters yielding  $A_e = -0.244 \pm 0.009$  and  $A_h = -0.331 \pm 0.007$ . This implies similar contributions of the  $L_5$  hole and the  $L_6$  electron to the  $L_{5-6}$  bleach.

Having established that electron transfer from photoexcited PbSe QDs to MB occurs, we study the influence of this process on the high energy bleach features X and Y. Figure 5a shows the TA image in the 375–600 nm probe range for 4.8 nm PbSe QDs with 5 MB molecules added per QD after photoexcitation at the band gap. Comparison with the TA image for QDs without MB in Figure 1a shows that addition of MB decreases the lifetime of both the X and Y bleach features, with a significantly shorter lifetime for X than for Y. The ground-state absorption spectrum of MB is shown in Figure S5. We observe

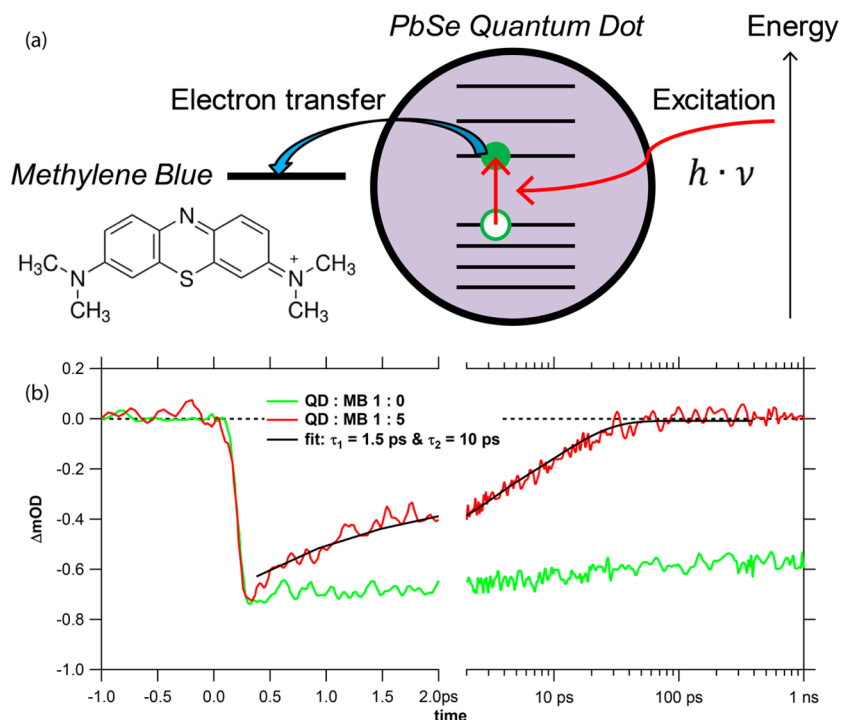


**Figure 4.** (a) Schematic of electron transfer from a photoexcited QD to MB. (b)  $L_{5-6}$  bleach transient for 4.8 nm PbSe QDs without MB (green) and with 5 MB molecules added per QD (red) after photoexcitation at the band gap. Fitting a biexponential function to the transient of QDs with MB yields time constants of 1.5 ps for electron transfer and 10 ps for electron–hole recombination.

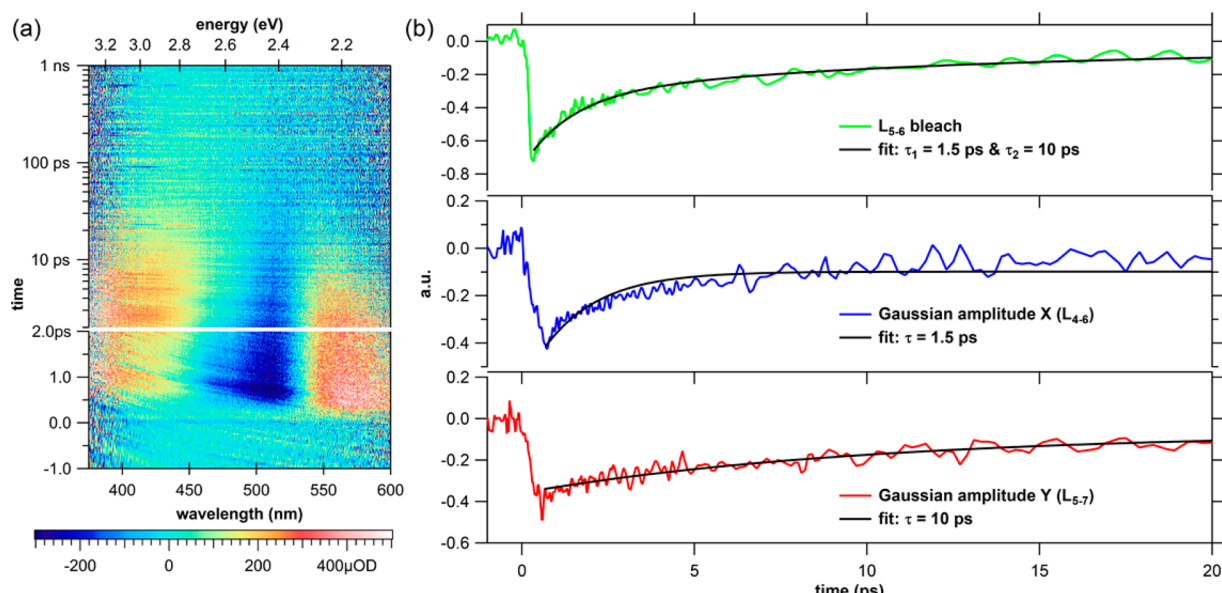


**Figure 5.** (a) TA image in the 375–600 nm probe range for 4.8 nm PbSe QDs with 5 MB molecules added per QD after photoexcitation at the band gap. (b) The  $L_{5-6}$  bleach transient and the time evolution of the fitted Gaussian amplitudes for the bleach features X and Y. The decay of the Gaussian amplitudes can be described by exponential functions with time constants of 1.5 and 10 ps, related to electron transfer from the QDs to MB and electron–hole recombination, respectively.

that the MB absorption feature occurs in the range 550–700 nm and does not influence the results shown in Figure 5a. We have observed a bleach of the MB absorption feature in TA experiments after electron transfer, but this is beyond the range of the data for the high energy transitions shown in Figure 5a.

The TA spectra at different times in Figure 5a can be described by fitting a sum of two Gaussians superimposed on a positive background that decreases linearly with photon energy,

similar to the TA spectra in Figure 2. The time-evolution of the fitted Gaussian amplitudes and the  $L_{5-6}$  bleach transient are shown in Figure 5b together with a global fit to all data. The transients are well described by exponential functions with time constants of 1.5 ps related to electron transfer and 10 ps related to electron–hole recombination. Any discrepancy between global fit and data we believe is caused by our phenomenal description of the background of PA and a slight overlap of the

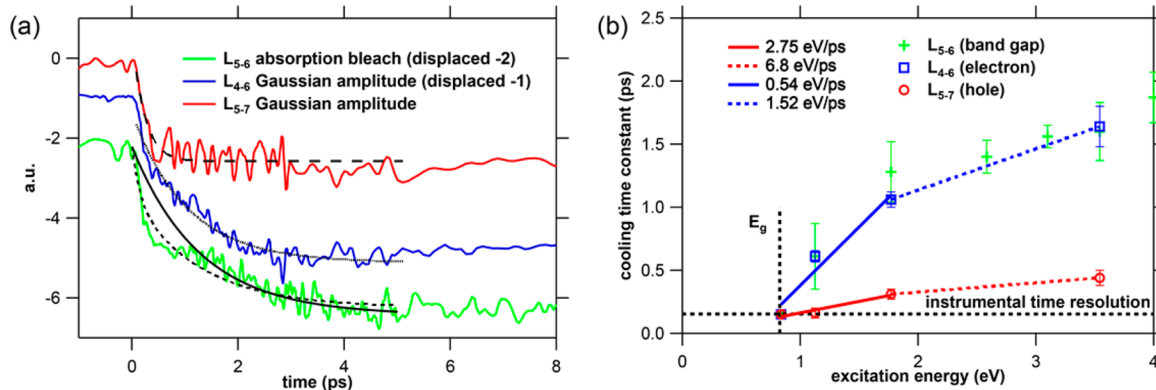


**Figure 6.** (a) Increase of the bleach of the L<sub>5-6</sub> ( $f(t)$ ), L<sub>4-6</sub>, and L<sub>5-7</sub> transitions for 4.8 nm PbSe QDs after 700 nm excitation during time. The transients can be described by a single exponential function with time constants discussed in the text. The L<sub>5-6</sub> transient is best described by a double exponential function with the time constants of the L<sub>4-6</sub> and L<sub>5-7</sub> transients. (b) Time constants describing the rise of the L<sub>5-6</sub> bleach and the rise of the Gaussian amplitudes of the L<sub>4-6</sub> and L<sub>5-7</sub> transitions using single exponential fit functions.

Gaussian bleach features X and Y that we are unable to fully disentangle. These results show that bleach feature X is caused by the presence of L<sub>6</sub>1S<sub>e</sub> electrons while bleach feature Y is caused by the presence of L<sub>5</sub>1S<sub>h</sub> holes and corroborate our assignment of X to the L<sub>4-6</sub> transition and Y to the L<sub>5-7</sub> transition.

The relaxation of hot charges in PbSe QDs to the band gap has been studied by monitoring the rise of the optical bleach at the band gap during time.<sup>37–39</sup> Since the bleach at the band gap is due to both the L<sub>6</sub> electron and the L<sub>5</sub> hole, it does not allow one to distinguish electron cooling from hole cooling. Interestingly, the L<sub>4-6</sub> and L<sub>5-7</sub> transitions give access to bleach features that depend either on the L<sub>6</sub> electron or the L<sub>5</sub> hole separately. Therefore, in addition to the rise of the optical bleach at the band gap, we also studied the kinetics of the bleach of the L<sub>4-6</sub> and L<sub>5-7</sub> transitions to independently characterize electron and hole cooling as a function of photoexcitation energy. This is done regardless of the exact mechanism involved in the cooling. We discuss some of the possible mechanisms later.

Relaxation of initially hot charges to the band gap yields the L<sub>5</sub>1S<sub>h</sub>-L<sub>6</sub>1S<sub>e</sub> exciton, which causes an increase of the L<sub>5-6</sub> bleach at the band gap during time. The peak due to this cold exciton in the ground-state absorption spectrum  $A$  can be described by a Gaussian function. The excited state absorption spectrum  $A^*$  of QDs containing at most one cold exciton is given by

$$\begin{aligned} A^* &= A + \Delta A \\ &= (1 - f(t))Ce^{-(E-E_0)^2/2\sigma^2} + f(t)\frac{3}{4}C \\ &\quad e^{-[E-(E_0-\delta E)]^2/2\sigma^2} \end{aligned} \quad (2)$$

where the parameters  $C$ ,  $E_0$ , and  $\sigma$  are known from a Gaussian fit to the ground-state absorption spectrum. The parameter  $f(t)$  is the fraction of QDs containing a relaxed L<sub>5-6</sub> exciton at time  $t$  after the pump laser pulse and  $\delta E$  is the shift in energy of the absorption peak of an excited QD. The factor 3/4 brings into account the 8-fold degeneracy of the L<sub>5-6</sub> exciton and the fact that the bleach results from both reduced absorption and stimulated emission. The L<sub>5-6</sub> bleach is then given by

$$\begin{aligned} \Delta A &= A^* - A \\ &= -f(t)Ce^{-(E-E_0)^2/2\sigma^2} + \frac{3}{4}f(t)Ce^{-[E-(E_0-\delta E)]^2/2\sigma^2} \end{aligned} \quad (3)$$

Fitting eq 3 to the TA spectrum yields  $f(t)$ .

Analogously, the amplitudes of the Gaussian functions describing the L<sub>4-6</sub> and L<sub>5-7</sub> transitions are obtained from fits as applied to the TA spectrum in Figure 2. A correct description of the positive TA background is imperative in this approach. As stated above, we expect the positive background to originate from a biexciton shift<sup>29</sup> and possibly intraband absorption. These depend on the excess energy of hot charges in the QD and will therefore change in a complex and unknown way during charge carrier relaxation. In the Supporting Information, we compare and discuss different models for the positive background in Figure S2. We choose to describe it by a function that decreases linearly with photon energy.

The fraction  $f(t)$  of QDs containing a relaxed L<sub>5-6</sub> exciton as well as the time-dependence of the Gaussian amplitudes of the L<sub>4-6</sub> and L<sub>5-7</sub> transitions obtained from the fits are shown in Figure 6a after excitation by a 700 nm (1.77 eV) pump laser pulse. We describe  $f(t)$  and the Gaussian amplitudes by a single exponential function and find time constants of 1.28, 1.04, and 0.34 ps for the increase of the bleach of the L<sub>5-6</sub>, L<sub>4-6</sub>, and L<sub>5-7</sub> transitions, respectively. We believe that any discrepancy between fit and data for the L<sub>4-6</sub> and L<sub>5-7</sub> transitions is caused by our inability to fully disentangle the two Gaussian features. We show these time constants for 4.8 nm PbSe QDs as a function of photoexcitation energy in Figure 6b. We have added a horizontal dashed line to indicate the instrumental time resolution of 180 fs and a vertical dashed line to mark the energy of the band gap.

Figure 6b shows that the time constant describing the rise of the L<sub>5-6</sub> bleach increases with excitation energy and reaches a value close to 2 ps for an excitation energy of 4 eV, in agreement with literature.<sup>11,13,39</sup> For excitation near the band gap energy, the time constant increases more rapidly with excitation energy than for higher energy excitation, consistent with the increased density of states higher above the band gap and correspondingly higher cooling rates.

The increase of the bleach of the L<sub>4-6</sub> transition with time is solely due to relaxation of electrons to the conduction band

edge state  $L_6$ . Analogously, the increase of the bleach of the  $L_{5-7}$  transition represents hole relaxation to the valence band edge state  $L_5$ . We observe from Figure 6b that the time constants describing the rise of the Gaussian amplitude of the  $L_{4-6}$  transition are similar to those describing the rise of the  $L_{5-6}$  bleach. In contrast, the time constants describing the rise of the Gaussian amplitude of the  $L_{5-7}$  transition are much shorter. These results show that hole cooling is much faster than electron cooling and that, due to hole cooling occurring largely within the time resolution of our measurement, the increase of the bleach of the  $L_{5-6}$  transition is mainly due to electron cooling.

The energy loss rate  $\gamma$ , for electrons or holes, is given by

$$\gamma = \frac{dE}{dt} = \left[ \frac{d\tau}{d(h\nu)} \right]^{-1} \quad (4)$$

where  $\tau$  is the cooling time constant and  $h\nu$  is the photoexcitation energy. Using eq 4, we find that  $\gamma$  is 0.54 eV/ps for electrons residing in energy levels near the band gap and 1.52 eV/ps at high energy. We note that the transition to higher energy loss rate occurs close to the  $\Sigma$ -point.<sup>27,40</sup> These values are comparable to the values recently calculated by Geiregat *et al.* for PbS QDs.<sup>27</sup> For holes, we however find a much higher  $\gamma$  of 2.75 eV/ps near the band gap and 6.8 eV/ps at high energy, while according to the calculations of Geiregat *et al.*, the energy loss rates for electrons and holes are similar.

As discussed above, we inferred from the data in Figure 4b that the contribution of the  $1S_h$  ( $L_5$ ) hole to the bleach of the  $L_{5-6}$  transition is comparable to that of the  $1S_e$  ( $L_6$ ) electron. If hole cooling is indeed faster than electron cooling, we expect the bleach of the  $L_{5-6}$  transition to appear with two different time constants. In Figure 6a, we showed  $f(t)$  as determined from the  $L_{5-6}$  transition using eq 3. Indeed, part of the bleach of the  $L_{5-6}$  transition appears within the 180 fs time resolution of our measurements, corresponding well to hole cooling. This instantaneous bleach is not caused by a Coulomb shift, because we correct for that using eq 3. On longer times, the bleach of the  $L_{5-6}$  transition increases with a time constant comparable to electron cooling. In fact, the bleach of the  $L_{5-6}$  transition is much better described by a biexponential function with the time constants of the rise of the Gaussian amplitudes of the  $L_{4-6}$  and  $L_{5-7}$  transitions (dashed line in Figure 6a) than by a single exponential function (solid black line in Figure 6a), in good agreement with the different cooling time constants presented here.

In the Supporting Information Figure S6, we show an identical analysis on 3.9 nm PbSe QDs. The exact cooling time constants are somewhat different from the cooling time constants for 4.8 nm PbSe QDs, but again show that hole cooling is much faster than electron cooling.

Thus, our results indicate that hole cooling is much faster than electron cooling. This is in contrast with the common expectation that electrons and holes behave similarly in Pb chalcogenide materials. It also contradicts recent tight-binding calculations that show that electron and hole energy loss rates are similar in bulk PbS, which should relate qualitatively well to energy loss rates in QDs high above the band gap.<sup>27</sup> In those calculations, carrier cooling was assumed to take place through LO phonon emission within the Fröhlich formalism. A critical parameter that determines the energy loss rate in these calculations is the density-of-states (DOS) in the valence band and conduction band. According to the tight-binding

calculations in ref 27, these densities-of-states are very similar for bulk PbS. However, pseudopotential calculations by Zunger *et al.* of the PbSe QD band structure relatively close to the band edges (these calculations are for excess carrier energies up to 0.4 eV) have suggested that the DOS in the valence band is higher than that in the conduction band.<sup>13,22</sup> There are also several experimental indications that this is indeed the case.<sup>18,23</sup> Well-above the band edges, the band structure of PbSe becomes less symmetric, even for DFT calculations of the bulk band structure. As stated above, the DFT calculations in Figure 3a show higher effective masses for holes at the  $L_4$  point than for electrons at the  $L_7$  point. This is equivalent to a higher density of states for holes at those energies. Therefore, we propose that a higher DOS in the valence band can explain the faster hole cooling that we observe.

The observed differences between electron and hole cooling rates imply that fast electron-to-hole Auger cooling is slower than direct cooling of the electron. In CdSe QDs, efficient electron Auger cooling is believed to equalize the 1P to 1S cooling rates of electrons and holes.<sup>41,42</sup> In that case, the electron scatters with a hole and the excess energy of the electron is transferred to the hole. Such electron Auger cooling is only efficient when the  $1P_e$ - $1S_e$  energy difference is resonant with the promotion of a 1S hole to a higher level.<sup>22</sup> In CdSe QDs, the valence band energy levels are so densely spaced that this is always the case. In PbSe QDs, the energy levels in the valence band are much less densely spaced,<sup>23</sup> and it seems likely that close to the band edge (e.g., for  $1P_e$  to  $1S_e$ ) electron Auger cooling is less efficient for that system, and electron and hole cooling rates can hence be dissimilar. At energies well above the band edges, it is unlikely that such absence of resonant transitions still occurs. Still we observe a significant disparity in electron and hole cooling rates at high excess energies, which implies that also at these energies direct electron cooling outcompetes Auger cooling.

It is conceivable that hole energy level differences could be resonant with ligand vibrational modes while electron energy level differences are not.<sup>10,43</sup> This could result in fast energy transfer to ligand vibrational modes and consequently faster hole relaxation near the band gap. For higher excess energy of charge carriers over the band gap energy, we however expect energy transfer to ligands to be of little influence as the spacing between energy levels is much smaller than typical ligand vibrational energies. From Figure 6b, we note that even at high energy, the energy loss rate is much higher for holes than for electrons. Possibly an additional relaxation pathway *via* the surface opens when charge carriers are given sufficiently high energy.<sup>16,17</sup> Our results indicate that this channel is mainly used by holes and not electrons.

Fast cooling of holes implies that utilizing the excess energy of hot holes, *e.g.*, for carrier multiplication or hot charge extraction, will be very challenging, while hot electrons will be easier to access. These results also shed new light on carrier multiplication in PbSe QDs as they suggest that carrier multiplication *via* electron scattering is likely much more efficient than *via* hole scattering.

## CONCLUSIONS

Band edge excitation of PbSe QDs leads to an optical bleach well above the band gap, which consists of two components superimposed on a background of photoinduced absorption. We assign the bleach to the  $L_{4-6}$  and  $L_{5-7}$  electronic transitions. Studies of the bleach at the band gap and at the  $L_{4-6}$  and  $L_{5-7}$

transitions allow us to determine separate rates for electron cooling and hole cooling. Our results show that hole cooling is much faster than electron cooling at all excitation energies. This implies that processes utilizing excess charge carrier energy such as carrier multiplication or hot carrier extraction will be much more efficient for electrons than for holes.

## METHODS

**PbSe QDs.** The 4.8 nm PbSe QDs were synthesized using the method described by Steckel *et al.*<sup>24</sup> In brief, 4.77 g of lead acetate tri hydrate (99.999%, Aldrich), 3.42 g of oleic acid (90%, Aldrich) and 13.14 g of 1-octadecene (90%, Aldrich) were placed into a flask and dried and reacted under vacuum for at least 2 h at 120 °C. A second mixture containing 1.12 g of selenium (99.999%, Alfa Aesar), 0.13 mL of diphenylphosphine (98%, Aldrich) and 14.87 mL of trioctylphosphine (90%, Fluka) was prepared. Subsequently, the lead mixture was heated to 180 °C under nitrogen and the selenium mixture was injected. The reaction was allowed to proceed for 20 s at 150 °C after which the reaction was quenched using 15 mL of butanol (99.8 anhydrous, Sigma-Aldrich). The crude synthesis mixtures were washed twice by precipitating with methanol, centrifugation and redispersion of the sediment in toluene. This resulted in particles with a diameter of 4.8 ± 0.3 nm. Other particle sizes were prepared by changing the reaction time after selenium injection.

**Hyperspectral TA Spectroscopy.** We studied electronic excited states in PbSe QDs using broadband pump–probe spectroscopy. The pure QD samples were dispersed in toluene in a 2 mm stirred quartz cuvette at a typical optical density of 0.05 at the band gap. The QD samples with Methylene Blue were dispersed in chloroform in a 2 mm stirred quartz cuvette at identical concentration.

Laser pulses of 180 fs were generated in a Yb:KGW oscillator (Light Conversion, Pharos SP) at 1028 nm and amplified. A small fraction of the 1028 nm fundamental beam was split off to generate the broadband probe spectrum in a sapphire (500–1600 nm) or CaF<sub>2</sub> (375–600 nm) crystal. The probe pulse was delayed up to 3 ns using an automated delay stage. The majority of the 1028 nm fundamental beam was used as a pump pulse after nonlinear frequency mixing in an OPA and second harmonics module (Light Conversion, Orpheus) to achieve wavelengths of 310–1500 nm. The pump and probe pulses overlap on the sample position under an angle of ~8°, after which the pump pulse is dumped and the probe light is led to a detector suitable for the probe spectrum selected (Ultrafast Systems, Helios). All shown data is corrected for dispersion by fitting a polynomial function to the solvent response.

In all experiments, the laser pump fluence was taken sufficiently low to prevent multiple photons being absorbed in a single QD. Assuming Poissonian statistics for photoexcitation, the probability  $P_N$  for a QD to contain  $N$  excitons is given by

$$P_N = \frac{e^{-\langle N \rangle} \langle N \rangle^N}{N!} \quad (5)$$

with the average number of excitons per QD equal to  $\langle N \rangle = J\sigma$ , where  $J$  is the laser pump fluence and  $\sigma$  is the photon absorption cross section. During the measurements, we take  $J$  low enough, so that  $P_{N \geq 2}$  is negligible, *i.e.*, below  $\langle N \rangle = 0.15$ , where  $P_2 = 0.01$  (~7%).

**DFT Calculations.** The calculation of the band structure of bulk PbSe was performed using the ADF/BAND program.<sup>30,32</sup> A cubic lattice with lattice constant of 6.12 Å was assumed in agreement with the experimental crystal structure. A single unit cell containing a lead and a selenide atom was considered with periodic boundary conditions. The calculation was performed using a spin-unrestricted TZ2P basis set with large frozen cores. The model exchange and correlation functional developed by Tran and Blaha (TB-mBJ) was used during the calculations.<sup>31</sup> This functional yields values for semiconductor band gaps that are close to the ones obtained by GW calculations at a fraction of the computational cost. Relativistic effects were included *via* a spin-orbit coupled ZORA (zeroth-order regular approximation).<sup>44</sup> The inclusion of spin-orbit coupling is essential

due to the presence of lead in the system. The effective masses of the different conduction and valence bands were obtained by numerical differentiation of their energies at the L-point as implemented in BAND.

## ASSOCIATED CONTENT

### S Supporting Information

The Supporting Information is available free of charge on the ACS Publications website at DOI: 10.1021/acsnano.5b05731.

Information on the positive background in the high energy TA spectrum; additional cooling time constants for 3.9 nm PbSe QDs; effective masses at the L-point (PDF)

## AUTHOR INFORMATION

### Corresponding Authors

\*E-mail: A.J.Houtepen@tudelft.nl.

\*E-mail: L.D.A.Siebbeles@tudelft.nl.

### Notes

The authors declare no competing financial interest.

## ACKNOWLEDGMENTS

This research was supported by the Dutch Foundation for Fundamental Research on Matter (FOM) in the programs “Hot Electrons in Cool Nanocrystals”, “Control over Functional Nanoparticle Solids” and “Designing Dirac Carriers in Semiconductor Honeycomb Superlattices”. This work has received financial support from the European Research Council (ERC) under grant agreement nr. 648433. We would like to thank Pieter Geiregat and Zeger Hens for fruitful discussions.

## REFERENCES

- Talapin, D. V.; Lee, J. S.; Kovalenko, M. V.; Shevchenko, E. V. Prospects of Colloidal Nanocrystals for Electronic and Optoelectronic Applications. *Chem. Rev.* **2010**, *110*, 389–458.
- Nozik, A. J. Quantum Dot Solar Cells. *Phys. E* **2002**, *14*, 115–120.
- Tisdale, W. A.; Williams, K. J.; Timp, B. A.; Norris, D. J.; Aydin, E. S.; Zhu, X. Y. Hot-Electron Transfer from Semiconductor Nanocrystals. *Science* **2010**, *328*, 1543–1547.
- Pandey, A.; Guyot-Sionnest, P. Hot Electron Extraction from Colloidal Quantum Dots. *J. Phys. Chem. Lett.* **2010**, *1*, 45–47.
- Yang, Y.; Rodriguez-Cordoba, W.; Xiang, X.; Lian, T. Strong Electronic Coupling and Ultrafast Electron Transfer Between PbS Quantum Dots and TiO<sub>2</sub> Nanocrystalline Films. *Nano Lett.* **2012**, *12*, 303–309.
- Padilha, L. A.; Stewart, J. T.; Sandberg, R. L.; Bae, W. K.; Koh, W. K.; Pietryga, J. M.; Klimov, V. I. Carrier Multiplication in Semiconductor Nanocrystals: Influence of Size, Shape and Composition. *Acc. Chem. Res.* **2013**, *46*, 1261–1269.
- Beard, M. C.; Luther, J. M.; Semonin, O. E.; Nozik, A. J. Third Generation Photovoltaics Based on Multiple Exciton Generation in Quantum Confined Semiconductors. *Acc. Chem. Res.* **2013**, *46*, 1252–1260.
- Smith, C.; Binks, D. Multiple Exciton Generation in Colloidal Nanocrystals. *Nanomaterials* **2014**, *4*, 19–45.
- Ten Cate, S.; Sandeep, C. S.; Liu, Y.; Law, M.; Kinge, S.; Houtepen, A. J.; Schins, J. M.; Siebbeles, L. D. A. Generating Free Charges by Carrier Multiplication in Quantum Dots for Highly Efficient Photovoltaics. *Acc. Chem. Res.* **2015**, *48*, 174–181.
- Pandey, A.; Guyot-Sionnest, P. Slow Electron Cooling in Colloidal Quantum Dots. *Science* **2008**, *322*, 929–932.
- Schaller, R. D.; Pietryga, J. M.; Goupalov, S. V.; Petruska, M. A.; Ivanov, S. A.; Klimov, V. I. Breaking the Phonon Bottleneck in

- Semiconductor Nanocrystals *via* Multiphonon Emission Induced by Intrinsic Nonadiabatic Interactions. *Phys. Rev. Lett.* **2005**, *95*, 196401.
- (12) Kambhampati, P. Hot Exciton Relaxation Dynamics in Semiconductor Quantum Dots: Radiationless Transitions on the Nanoscale. *J. Phys. Chem. C* **2011**, *115*, 22089–22109.
- (13) An, J. M.; Califano, M.; Franceschetti, A.; Zunger, A. Excited-State Relaxation in PbSe Quantum Dots. *J. Chem. Phys.* **2008**, *128*, 164720.
- (14) Miaja-Avila, L.; Tritsch, J. R.; Wolcott, A.; Chan, W. L.; Nelson, C. A.; Zhu, X. Y. Direct Mapping of Hot-Electron Relaxation and Multiplication Dynamics in PbSe Quantum Dots. *Nano Lett.* **2012**, *12*, 1588–1591.
- (15) Cho, B.; Peters, W. K.; Hill, R. J.; Courtney, T. L.; Jonas, D. M. Bulklike Hot Carrier Dynamics in Lead Sulfide Quantum Dots. *Nano Lett.* **2010**, *10*, 2498–2505.
- (16) Ellingson, R. J.; Blackburn, J. L.; Yu, P. R.; Rumbles, G.; Micic, O. I.; Nozik, A. J. Excitation Energy Dependent Efficiency of Charge Carrier Relaxation and Photoluminescence in Colloidal InP Quantum Dots. *J. Phys. Chem. B* **2002**, *106*, 7758–7765.
- (17) Ellingson, R. J.; Blackburn, J. L.; Nedeljkovic, J.; Rumbles, G.; Jones, M.; Fu, H. X.; Nozik, A. J. Theoretical and Experimental Investigation of Electronic Structure and Relaxation of Colloidal Nanocrystalline Indium Phosphide Quantum Dots. *Phys. Rev. B: Condens. Matter Mater. Phys.* **2003**, *67*, 075308.
- (18) Trinh, M. T.; Houtepen, A. J.; Schins, J. M.; Piris, J.; Siebbeles, L. D. A. Nature of the Second Optical Transition in PbSe Nanocrystals. *Nano Lett.* **2008**, *8*, 2112–2117.
- (19) Schins, J. M.; Trinh, M. T.; Houtepen, A. J.; Siebbeles, L. D. A. Probing Formally Forbidden Optical Transitions in PbSe Nanocrystals by Time- and Energy-Resolved Transient Absorption Spectroscopy. *Phys. Rev. B: Condens. Matter Mater. Phys.* **2009**, *80*, 035323.
- (20) Trinh, M. T.; Sfeir, M. Y.; Choi, J. J.; Owen, J. S.; Zhu, X. Y. A Hot Electron-Hole Pair Breaks the Symmetry of a Semiconductor Quantum Dot. *Nano Lett.* **2013**, *13*, 6091–6097.
- (21) Ellingson, R. J.; Beard, M. C.; Johnson, J. C.; Yu, P.; Micic, O. I.; Nozik, A. J.; Shabaev, A.; Efros, A. L. Highly Efficient Multiple Exciton Generation in Colloidal PbSe and PbS Quantum Dots. *Nano Lett.* **2005**, *5*, 865–871.
- (22) An, J. M.; Franceschetti, A.; Dudiy, S. V.; Zunger, A. The Peculiar Electronic Structure of PbSe Quantum Dots. *Nano Lett.* **2006**, *6*, 2728–2735.
- (23) Liljeroth, P.; Zeijlmans van Emmichoven, P. A.; Hickey, S. G.; Weller, H.; Grandidier, B.; Allan, G.; Vanmaekelbergh, D. Density of States Measured by Scanning-Tunneling Spectroscopy Sheds New Light on the Optical Transitions in PbSe Nanocrystals. *Phys. Rev. Lett.* **2005**, *95*, 086801.
- (24) Steckel, J. S.; Yen, B. K.; Oertel, D. C.; Bawendi, M. G. On the Mechanism of Lead Chalcogenide Nanocrystal Formation. *J. Am. Chem. Soc.* **2006**, *128*, 13032–13033.
- (25) Wehrenberg, B. L.; Wang, C. J.; Guyot-Sionnest, P. Interband and Intraband Optical Studies of PbSe Colloidal Quantum Dots. *J. Phys. Chem. B* **2002**, *106*, 10634–10640.
- (26) Kigel, A.; Brumer, M.; Maikov, G. I.; Sashchiuk, A.; Lifshitz, E. Thermally Activated Photoluminescence in Lead Selenide Colloidal Quantum Dots. *Small* **2009**, *5*, 1675–1681.
- (27) Geiregat, P.; Delerue, C.; Justo, Y.; Aerts, M.; Spoor, F. C. M.; Van Thourhout, D.; Siebbeles, L. D. A.; Allan, G.; Houtepen, A. J.; Hens, Z. A Phonon Scattering Bottleneck for Carrier Cooling in Lead Chalcogenide Nanocrystals. *ACS Nano* **2015**, *9*, 778–788.
- (28) Trinh, M. T.; Houtepen, A. J.; Schins, J. M.; Hanrath, T.; Piris, J.; Knulst, W.; Goossens, A. P. L. M.; Siebbeles, L. D. A. In Spite of Recent Doubts Carrier Multiplication Does Occur in PbSe Nanocrystals. *Nano Lett.* **2008**, *8*, 1713–1718.
- (29) Geiregat, P.; Houtepen, A. J.; Justo, Y.; Grozema, F. C.; Van Thourhout, D.; Hens, Z. Coulomb Shifts upon Exciton Addition to Photoexcited PbS Colloidal Quantum Dots. *J. Phys. Chem. C* **2014**, *118*, 22284–22290.
- (30) SCM BAND, VU University: Amsterdam, <http://www.scm.com>, 2014, accessed July 2015.
- (31) Tran, F.; Blaha, P. Accurate Band Gaps of Semiconductors and Insulators with a Semilocal Exchange-Correlation Potential. *Phys. Rev. Lett.* **2009**, *102*, 226401.
- (32) te Velde, G.; Baerends, E. J. Precise Density-Functional Method for Periodic Structures. *Phys. Rev. B: Condens. Matter Mater. Phys.* **1991**, *44*, 7888–7903.
- (33) Kohn, S. E.; Yu, P. Y.; Petroff, Y.; Shen, Y. R.; Tsang, Y.; Cohen, M. L. Electronic Band-Structure and Optical Properties of PbTe, PbSe and PbS. *Phys. Rev. B* **1973**, *8*, 1477–1488.
- (34) Allan, G.; Delerue, C. Confinement Effects in PbSe Quantum Wells and Nanocrystals. *Phys. Rev. B: Condens. Matter Mater. Phys.* **2004**, *70*, 245321.
- (35) Huang, J.; Huang, Z.; Yang, Y.; Zhu, H.; Lian, T. Multiple Exciton Dissociation in CdSe Quantum Dots by Ultrafast Electron Transfer to Adsorbed Methylene Blue. *J. Am. Chem. Soc.* **2010**, *132*, 4858–4864.
- (36) Yang, Y.; Rodriguez-Cordoba, W.; Lian, T. Ultrafast Charge Separation and Recombination Dynamics in Lead Sulfide Quantum Dot-Methylene Blue Complexes Probed by Electron and Hole Intraband Transitions. *J. Am. Chem. Soc.* **2011**, *133*, 9246–9249.
- (37) Harbold, J. M.; Du, H.; Krauss, T. D.; Cho, K. S.; Murray, C. B.; Wise, F. W. Time-Resolved Intraband Relaxation of Strongly Confined Electrons and Holes in Colloidal PbSe Nanocrystals. *Phys. Rev. B: Condens. Matter Mater. Phys.* **2005**, *72*, 195312.
- (38) Schaller, R. D.; Agranovich, V. M.; Klimov, V. I. High-Efficiency Carrier Multiplication Through Direct Photogeneration of Multi-Excitons *via* Virtual Single-Exciton States. *Nat. Phys.* **2005**, *1*, 189–194.
- (39) Aerts, M.; Spoor, F. C. M.; Grozema, F. C.; Houtepen, A. J.; Schins, J. M.; Siebbeles, L. D. A. Cooling and Auger Recombination of Charges in PbSe Nanorods: Crossover from Cubic to Bimolecular Decay. *Nano Lett.* **2013**, *13*, 4380–4386.
- (40) Koole, R.; Allan, G.; Delerue, C.; Meijerink, A.; Vanmaekelbergh, D.; Houtepen, A. J. Optical Investigation of Quantum Confinement in PbSe Nanocrystals at Different Points in the Brillouin Zone. *Small* **2008**, *4*, 127–133.
- (41) Hendry, E.; Koeberg, M.; Wang, F.; Zhang, H.; Donega, C. D.; Vanmaekelbergh, D.; Bonn, M. Direct Observation of Electron-to-Hole Energy Transfer in CdSe Quantum Dots. *Phys. Rev. Lett.* **2006**, *96*, 057408.
- (42) Efros, A. L.; Kharchenko, V. A.; Rosen, M. Breaking the Phonon Bottleneck in Nanometer Quantum Dots: Role of Auger-Like Processes. *Solid State Commun.* **1995**, *93*, 281–284.
- (43) Guyot-Sionnest, P.; Wehrenberg, B.; Yu, D. Intraband Relaxation in CdSe Nanocrystals and the Strong Influence of the Surface Ligands. *J. Chem. Phys.* **2005**, *123*, 074709.
- (44) Philipsen, P. H. T.; Baerends, E. J. Relativistic Calculations to Assess the Ability of the Generalized Gradient Approximation to Reproduce Trends in Cohesive Properties of Solids. *Phys. Rev. B: Condens. Matter Mater. Phys.* **2000**, *61*, 1773–1778.